frontiers | Frontiers in Sensors

TYPE Original Research
PUBLISHED 18 November 2022
DOI 10.3389/fsens.2022.1040542



OPEN ACCESS

EDITED BY
Massimo Mastrangeli,
Delft University of Technology,
Netherlands

REVIEWED BY
Benoit Scheid,
Université libre de Bruxelles, Belgium
Jinkee Lee,
Sungkyunkwan University, South Korea

*CORRESPONDENCE
Chang-Soo Lee,
rhadum@cnu.ac.kr

SPECIALTY SECTION
This article was submitted to Lab-on-a-Chip Devices,
a section of the journal
Frontiers in Sensors

RECEIVED 09 September 2022
ACCEPTED 07 November 2022
PUBLISHED 18 November 2022

CITATION
Daradmare S, Kim JS, Ganguly R and Lee C-S (2022), One-step on-chip microfluidic synthesis of the hybrid capsules using aqueous two-phase system.
*Front. Sens.* 3:1040542.
doi: 10.3389/fsens.2022.1040542



# One-step on-chip microfluidic synthesis of the hybrid capsules using aqueous two-phase system

Sneha Daradmare, Jae Seong Kim, Reya Ganguly and Chang-Soo Lee*

Department of Chemical Engineering and Applied Chemistry, Chungnam National University, Yuseong-gu, South Korea

Hydrogel capsules synthesized by conventional water-in-oil emulsion systems are the less preferred choice for biomedical applications due to the use of oils and surfactants. An aqueous two-phase system (ATPS), which allows the formation of water-in-water emulsion, is considered a green alternative and therefore has been explored a lot for its application in the biomedical field. Herein, we present the synthesis of hydrogel capsules using a set-up consisting of a pneumatic valve integrated with the ATPS microfluidic system. In this arrangement, at first, a pneumatic valve facilitates the generation of the droplets of one aqueous system i.e. sodium alginate (SA) containing dextran solution into another aqueous phase comprising polyethylene glycol solution. The present approach allows good control over droplet generation by tuning the pressure of the pneumatic valve and the flow rates of the core and middle phases. The synthesis of hybrid capsules within the microfluidic device is carried out mainly by using the interfacial complexation of oppositely charged polyelectrolytes, chitosan with SA *via* electrostatic interactions. The interfacial complexed SA and chitosan hydrogel capsules were collected *via* the settling collection method, which ensures the retaining of the shape of the hybrid capsules. The morphological properties of as-synthesized droplets and hybrid capsules were examined *via* optical microscopy. The hydrogel capsules show good encapsulation capability for the magnetic particles. Even though this study mainly focuses on the synthesis part, we anticipate that the proposed approach will enable the encapsulation of cells within the hybrid capsules as well as enhance the cell adhesion on the surface of the hydrogel capsules hence, these hydrogel capsules can find the potent application in the biomedical engineering.

KEYWORDS

**hybrid capsules, aqueous two-phase system, microfluidic system, interfacial complexation, electrostatic interactions**

# 1 Introduction

An aqueous two-phase system (ATPS) is an immiscible water-based solution system that is formed when two dissimilar solutes, polymers, or salts of high concentrations are dissolved in the aqueous media (Albertsson, 1970). The traditional purpose of ATPS was to use them in the separation and purification of various biological and non-biological materials (Ferreira-Faria et al., 2020; Assis et al., 2021). Later on, in the 20th century, researchers have begun exploiting the utility of ATPS in microfluidic systems to generate water-in-water (w/w) emulsion droplets (Choi et al., 2007; Ziemecka et al., 2011; Shum et al., 2012; Hann et al., 2017). However, the major challenge of using ATPS in microfluidic systems is the ultralow interfacial surface tension between two aqueous phases resulting in unstable droplets formation (Sauret et al., 2012; Azizian et al., 2019; Beldengrün et al., 2020). But, recent investigations have shown numerous ways for example, passive and active methods to stabilize the droplets within the microfluidic devices (Chao et al., 2020; Daradmare et al., 2022). The successful generation of w/w droplets within microfluidic devices provides a great opportunity to utilize these uniform-sized droplets in various applications, such as biological hosts, reactors, and templates in the synthesis of biomaterials (Chao et al., 2020). Howsoever, the stabilization of these w/w emulsion droplets remains challenging.

Interestingly, researchers have attempted several strategies for the stabilization of w/w emulsion droplets that prevent droplet coalescence (Chao et al., 2020; Daradmare et al., 2022). Most of the strategies such as the use of synthesizing customized macromolecular polymers and different kinds of colloidal particles have been employed in bulk ATPS emulsification to stabilize w/w emulsion droplets (Buzza et al., 2013; Binks et al., 2017; Dumas et al., 2021). However, in recent times, the use of polyelectrolyte (PE) complexation (PEC) at the water-water interface has been the only alternative employed in microfluidic devices to stabilize w/w droplets leading to the formation of hydrogel capsules (Hann et al., 2016; Ma et al., 2016). In this case, two PEs disperse in one or the other phase, for example, PE1 in one aqueous phase (droplet-forming phase) and PE2 in another aqueous phase (continuous phase), meet at the droplet interface during the formation of the droplets within the microfluidic device and form a robust solid shell *via* attractive electrostatic interactions.

The foremost function of hydrogel capsules (biocompatible) is the encapsulation and controlled release of chemically sensitive reagents that found their applications in various fields including the targeted drug delivery of pharmaceutical actives and live cell encapsulation, with applications ranging from the fundamental study of microbes to the development of artificial organs (Hann et al., 2016). Several classical ways have been used to fabricate hydrogel capsules in past years are listed somewhere (Perro et al., 2022). Most of which use chemical reactions or physical interactions in oil-water media. The reagents such as oils and/or surfactants may reduce the biocompatibility of the hydrogel capsules, and may have a toxic interaction with encapsulating cells or proteins, or other biological entities (Hann et al., 2016; Zhang et al., 2016). Therefore, the microfluidic device *via* the PEC-based stabilization technique offers a promising approach to the fabrication of uniform-sized hydrogel capsules. This approach offers several advantages including rapid complexation, diverse materials selection, and scalable single-step processing (Hann et al., 2017). The PE/PE hydrogel capsules have flexible and elastic membranes that can support pressure differences, as evidenced by their ability to wrinkle and expand under osmotic stresses. The polyelectrolyte complex layer is also permeable, allowing chemical exchange between the interior and exterior of the microcapsule. Finally, these capsules are stimuli-responsive; the electrostatic interactions can be modulated using external stimuli such as pH and ionic strength (Hann et al., 2017). And when these hydrogel capsules form by an ATPS, the system offers some extra advantages such as providing a highly favorable environment for sensitive biological or chemical cargo. In addition, no extra washing steps are required, so the cargo can be loaded into the emulsion templates at the time of the fabrication of PEC-based capsules. This feature is highly desirable for loading expensive pharmaceutical reagents because of lower reagent consumption (Navi et al., 2020).

To the best of our knowledge, to this date, there are only a fingerful of work has been studied on the fabrication of PECs within a microfluidic device using ATPS (Zhang et al., 2016; Zou et al., 2019; Liu et al., 2020; Navi et al., 2020; Wang et al., 2020). Zhang et al. reported the fabrication of PEC-based capsules using ATPS droplets generated in a glass capillary microfluidic device. They used polyelectrolyte microcapsules (PEMCs) for the encapsulation and release of proteins (Zhang et al., 2016). Recently, Zou et al. used the same platform a glass capillary microfluidic device along with a mechanical wave generator, and added silica nanoparticles to the shell material to generate PEC-based capsules. They reported successful encapsulation and release of the enzyme trypsin (Zou et al., 2019). Further, the pneumatic valve-integrated microfluidic device was employed to fabricate PEC-based capsules that provided a robust platform to engineer human islet organoids (Liu et al., 2020; Wang et al., 2020). In the same year, Navi et al. fabricated the magnetic PEMCs using an ATPS-integrated microfluidic device (Navi et al., 2020).

Our work is inspired and motivated by previous works, and is a result of the integration of ideas from these previously reported platforms for the generation of PEC-based capsules (Zhang et al., 2016; Zou et al., 2019; Liu et al., 2020; Navi et al., 2020; Wang et al., 2020). However, developing a new platform based on the integration of a new collection method is in the manuscript. In our work, we present a one-step on-chip microfluidic approach for the fabrication of the hybrid capsules using an aqueous two-phase system (ATPS) based on the interfacial complexation of

two oppositely charged PEs: polycations of chitosan and polyanions of sodium alginate (SA). In this present study, we employ a pneumatic valve to generate the w/w droplets. We found that the factors such as the pressure of the valve, and flow rates of the core and middle phases tune the size of the w/w droplets. Further, we compared the conventional vertical tubing collection method with the settling collection method for collecting the as-fabricated capsules and found that the settling collection method involves the controlled release of the as-generated capsules within the microfluidic chip from the bottom outlet that maintains their regular size. We observed that the flow rate of the core phase affects the capsules' size. We also demonstrated our capsules are capable of encapsulating the magnetic particles.

# 2 Materials and methods

## 2.1 Materials

Dextran (500 kDa, Alfa Aesar), PEG (20 kDa, Sigma Aldrich), sodium alginate (250 cps, Sigma Aldrich), chitosan (>400 cps, Sigma Aldrich), glacial acetic acid (≥99%, Sigma Aldrich), sodium hydroxide (95%, Jin Chemical Pharmaceutical Co., Ltd.), fluorescein isothiocyanate isomer 1 (FITC, 90%, Sigma Aldrich), ferric oxide, $Fe_2O_3$ nanoparticles (<50 nm average size, Sigma Aldrich) were used for the process of the hydrogel capsules' synthesis. Sodium phosphate dibasic (99%, Sigma Aldrich), potassium phosphate monobasic (99%, Sigma Aldrich), sodium chloride (99.5%, Sigma Aldrich), potassium chloride (99%, Duksan Pharmaceutical Co., Ltd.) were used to prepare the PBS solution. Polydimethylsiloxane and the curing agent (Sylgard 184, Dow Corning, MI, United States), and photoresist (SU-8 3035, Microchem Corp, Newton, MA) were used for the fabrication of the microfluidic chip. Methanol (90%, Samchun Pure Chemicals Co., Ltd.) and DI water were used as solvents. All reagents are used as received.

## 2.2 Fabrication of the microfluidic device

The microfluidic chip was fabricated by a standard soft lithography method (Jang et al., 2016; Jin et al., 2021). The desired outlay of the microfluidic device was made by using AutoCAD software. Further, the master mold (patterned silicon wafer) of the required height was prepared by a photolithography method using SU-8 3035 photoresist (Jang et al., 2016; Jin et al., 2021). The PDMS prepolymer and the curing agent at a weight ratio of 10:1 were mixed and degassed using a vacuum pump at room temperature to remove the air bubbles. The homogeneous mixture was then poured over the master mold and thermally cured at 65°C for 12 h in a convection oven to form the structure at the bottom of the cured PDMS sheet (PDMS replica). The structured PDMS replica was carefully peeled off the mold without damaging the structure. The inlet and outlet ports on the structured PDMS replica were produced by punching holes with a biopsy punch of diameter (ϕ) 0.75 mm and 1.5 mm, respectively. As we collected the hybrid capsules *via* the settling collection method, for this system, the outlet port of 2 mm ϕ on a glass slide was made using a glass drilling machine (KITECH Device, Sherline Model 2010; United States). Subsequently, the structured PDMS replica that has the inlet and outlet ports was bound with a plain PDMS slab (for the vertical tubing collection method), and the structured PDMS replica that has only inlet ports was bound with a glass slide with an outlet port (for settling collection method) after oxygen-plasma treatment for about 1–2 min, then the aligned microfluidic device was kept in an oven at 100°C for at least 2 h to stabilize the bond strength.

The dimensions of the final fabricated microfluidic channels are as follows; the height of the microfluidic channels is 100 ± 5.4 μm. In addition, the length and width of the pneumatic valve are 800 ± 7.87 μm and 200 ± 3.45 μm, respectively, which could control the generation of the droplets. The widths of the inlet channels, outlet channel along with serpentine channel are 100 ± 2.13 μm and 200 ± 3.10 μm, respectively.

## 2.3 Fabrication of hybrid capsules

The ATPS-integrated microfluidic system was composed of two polymer solutions, 15 wt% dextran (DEX) and 17 wt% PEG were dissolved in DI water. The core phase consisting of different amounts of SA was dissolved in the 15 wt% DEX solution to form the core flow solution of different concentrations. The middle phase was the pure solution of 17 wt% PEG. Different amounts of chitosan were dissolved in the 17 wt% PEG solution, pH was adjusted to five by acetic acid to form a homogeneous chitosan solution (of different concentrations) as the shell flow solution. The solutions of the core, middle and shell phases were loaded in the syringes (KOVAX, South Korea) and pumped into the inlets of the microfluidic device by using syringe pumps (PHD ULTRA, Harvard Apparatus, United States). The pneumatic valve was located near the first flow-focusing junction which squeezes and opens (a switching cycle) the main channel with the help of the carrier nitrogen gas leading to the generation of droplets at the end of a switching cycle. A nitrogen gas provided to the pneumatic valve was controlled by the pressure regulator gauge. The period of a switching cycle was 1.0 Hz and was kept constant throughout our experiment. We identified the shape of the signal was sinusoidal. Once then, droplets generated by the pneumatic valve were carried toward the second flow-focusing junction with the help of the middle phase where the droplets meet shell flow leading to the capsules' fabrication. At the second flow-focusing junction, the electrostatic complexation between oppositely charged PEs, SA, and chitosan occurred. The as-fabricated capsules were collected

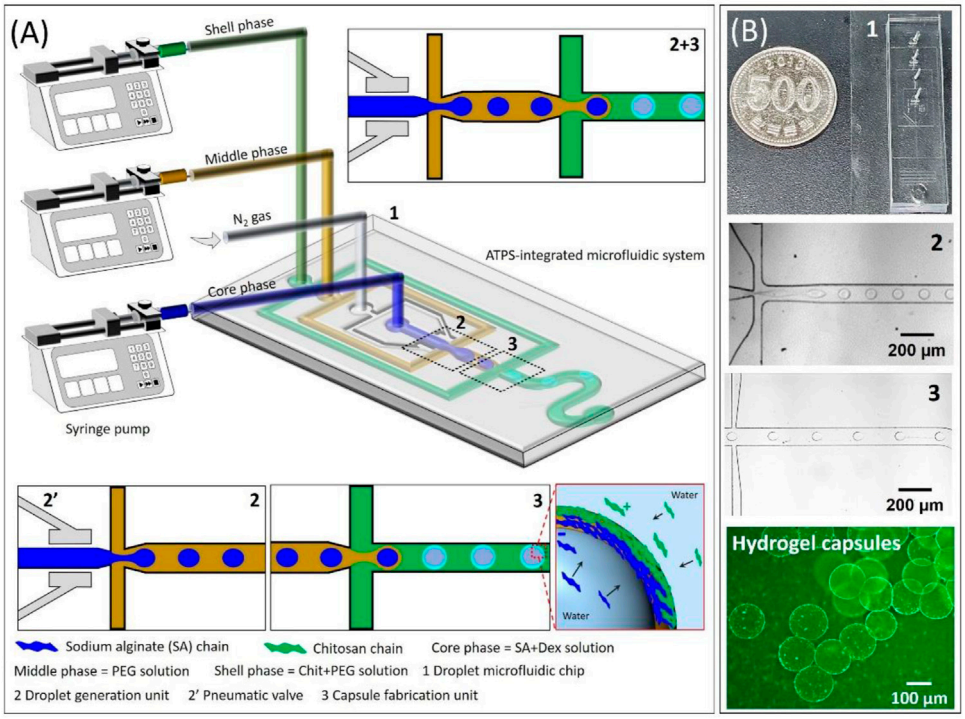


FIGURE 1
**(A)** Schematic illustration of oil-free all-aqueous-phase droplet microfluidic system platform to fabricate hydrogel capsules *via* interfacial complexation between oppositely charged polyelectrolytes, and **(B)** corresponding digital photograph and optical microscope images highlight different sections of the microfluidic chip and as-fabricated hydrogel capsules.

in the collection chamber containing PBS solution and characterized using an inverted microscope (TE-2000U, Nikon, Japan) equipped with a high-resolution CCD camera (Coolsnap cf, Photomaterials, AZ, United States). The software ImagePro (Media Cybernetics, MD, United States) was used to obtain images. The size of the capsules was measured using ImageJ (NIH, National Institutes of Health, MD, United States).

## 2.4 Synthesis of FITC labeled chitosan

To confirm the complexation at the interface of the hybrid capsules, FITC was chosen for labeling the chitosan. The labeling of chitosan with FITC occurred by the conjugation of the primary group of the amine of the chitosan with the isothiocyanate group of FITC (Sharma et al., 2012). FITC-labeled chitosan was prepared according to the reported literature (Liu et al., 2020; Wang et al., 2020). Briefly, 0.5 g chitosan was dissolved in the solution of 50 ml acetic acid (0.1 M). 50 ml methanol was then added to the homogeneous chitosan solution followed by the addition of 25 ml methanol containing FITC (2 mg/ml). The mixture solution was stirred for 3 h in the dark at room temperature. After the reaction, 0.2 M NaOH solution was added to the final mixture solution until the pH reached 9–10 to obtain the precipitation of FITC- chitosan. The FITC-chitosan precipitate was collected after the centrifugation (LABOGENE 2236R, LS Industrial Systems, South Korea) at 4°C at 15000 rpm for 10 min. Free FITC was separated by repeated washing with the mixture of methanol/water (7:3 volume ratio) and centrifuged until no fluorescence was detected in the supernatant. The FITC- chitosan was then dialyzed using a dialysis bag (cut-off MW = 6–8 kD, Spectrum Laboratories, Inc., United States) against DI water for 3 days in the dark with the exchange of fresh DI water daily. The dialyzed FITC-chitosan was freeze-dried in a lyophilizer (EYELA FDU-2200, Tokyo Rikakikai Co., Ltd., Japan) for about 3 days to obtain a dry powder. Further, the dry powder of FITC-chitosan was used for the subsequent experiments.

# 3 Results and discussion

## 3.1 Design and manipulation of ATPS droplet microfluidic platform

The design of our microfluidic device includes three inlets, a pneumatic valve, the two flow-focusing junctions, one is for

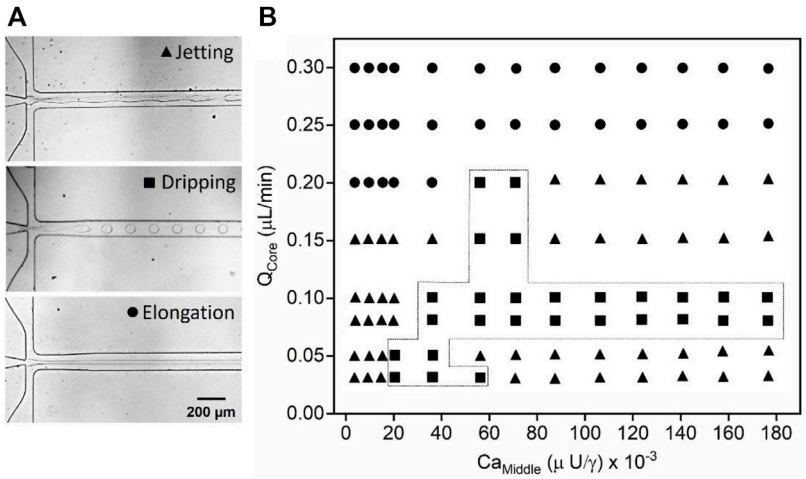


FIGURE 2
W/w droplet generation in the microfluidic device. **(A)** Optical microscope images of the different flow regimes observed during the droplet generation at the flow-focusing junction, and **(B)** phase diagram plotted as a function of the $Q_{Core}$ and capillary number (based on $Q_{Middle}$) ($Ca_{Middle}$) showing different flow regimes such as jetting, dripping, and elongation. The pneumatic valve at a pressure of 0.35 MPa was used for all the experiments.

droplet generation and another is for the fabrication of capsules and a serpentine channel provided more time for the capsules to undergo interfacial complexation to form a strong solid interface which was then connected with an outlet for the capsules collection as can be seen in Figure 1A. In this present work, SA/DEX, PEG, and chitosan/PEG solutions were employed as core, middle, and shell phase solutions. In the past, because of the ultralow interfacial tension between water-water phases, researchers have tried active-microfluidic methods that involve the use of external perturbation to generate the droplets (Chao et al., 2020; Daradmare et al., 2022). A pneumatic valve that converts mechanical energy into surface energy partially addressed the limitation of ultralow interfacial tension between water-water phases (Wang et al., 2020). A pneumatic valve compresses and opens the microchannel of the core phase periodically when the carrier nitrogen gas goes in and out of the microchannel of the valve that activating the generation of the droplets at the end of the one complete valve cycle. These ATPS droplets served as templates for the capsules' fabrication. The fabrication of capsules is mainly based on the interfacial complexation of PEs, negatively charged SA and positively charged chitosan. Specifically, the ATPS droplets containing SA generated at the first flow-focusing junction were then carried toward the second flow-focusing junction where they meet with the shell phase containing chitosan. Because of the concentration gradient, SA and chitosan diffuse from the droplets, and shell phase, respectively toward the middle phase and form a complexation *via* electrostatic interactions (Zou et al., 2019; Liu et al., 2020; Wang et al., 2020). It was observed that the hydrogel capsules swelled immediately because of the water uptake in the microcapsule while the shell structure was intact when they were transferred to the PBS medium (their sizes can be compared from Figure 1B).

## 3.2 Controllable generation of ATPS droplets

Figure 2 presents a phase diagram showing the different flow regimes over a wide range of the flow rates of the core phase ($Q_{Core}$) and capillary number (based on $Q_{Middle}$) ($Ca_{Middle}$). To conduct this study, 15 wt% DEX, and 17 wt% PEG solutions were used as core and middle phases, respectively. The pneumatic valve at the pressure of 0.35 MPa was used to generate the droplets at the first flow-focusing junction. We observed three typical flow patterns in the junction such as unstable droplets, monodisperse droplets, and thread-like continuous flow. The optical microscope images represent the three different flow regimes in the flow-focusing junctions as shown in Figure 2A. As can be seen in Figures 2A,B phase diagram is mainly divided into three flow regimes: jetting, dripping, and elongation. Jetting is the regime where the breaking of the droplets happens from the elongated thread of the core phase due to Rayleigh-Plateau instability resulting in polydisperse droplets (Kumar et al., 2020). The dripping regime yields droplets at the flow-focusing junction that are highly monodisperse which is the most wanted regime in the droplet generation process to manipulate the size of the droplets. An elongation regime is the continuous thread-like form of the core phase flowing in the middle phase (Kim et al., 2018).

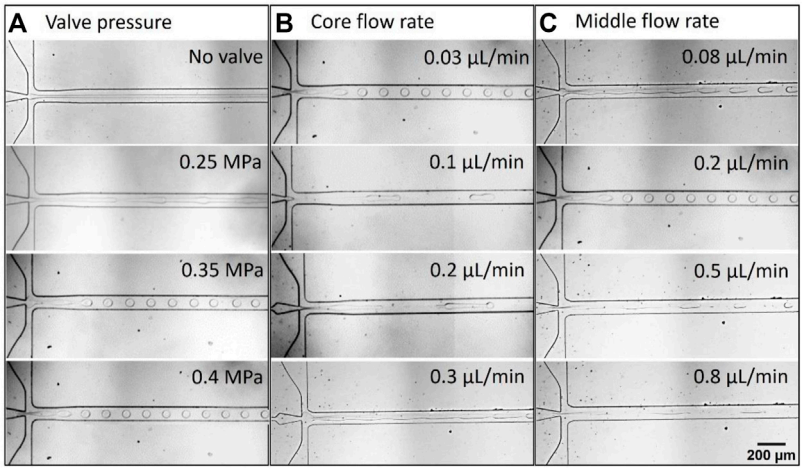


FIGURE 3
Droplet generation snapshots; the influence of the different operating parameters on the droplets' generation such as; **(A)** pressures of the valve at the constant $Q_{Core}$ and $Q_{Middle}$ of 0.03 and 0.2 µL/min, respectively, **(B)** $Q_{Core}$ at the constant $Q_{Middle}$ of 0.2 µL/min and 0.35 MPa valve pressure, and **(C)** $Q_{Middle}$ at the constant $Q_{Core}$ of 0.03 µL/min and 0.35 MPa valve pressure.

The formation of the flow at the flow-focusing junction is mostly determined by a force balance between the viscous stress and the surface tension stress (Kim et al., 2018). Therefore, the dimensionless number *Ca* ($Ca = \mu U/\gamma$) comes into existence, where, *U* ($U = Q_{Middle}/A$, where, *A* is the cross-section area microfluidic channel) is the velocity of the middle phase, $\mu$ indicates the viscosity of the middle phase (35 ± 1.98 cP), measured by a Brookfield rheometer (RC, United States), and $\gamma$ represents the interfacial tension (40 ± 4.34 µn/m) between the core and middle phases measured by an interfacial tensiometer (Attension, United States), overall, the *Ca* was controlled by varying $Q_{Middle}$. A phase diagram is important in understanding droplet generation, plotting various flow rates of the core phase (0.03–0.2 µL/min) as a function of different $Ca_{Middle}$ ranging from 0.0025 to 0.176. It was observed that the jetting and dripping regimes appear at low flow rates of the core phase over the wide range of $Ca_{Middle}$ as shown in Figure 2. The jetting regime is seen for $0.03 < Q_{Core} < 0.2$ µL/min and $0.0025 < Ca_{Middle} < 0.176$. However, the monodisperse w/w droplets are generated only within the limited regime. The first transition from jetting to the dripping regime occurs at $Ca_{Middle} \approx 0.018$ for $Q_{Core} = 0.03$ µL/min. In this regime, shear forces from the middle phase are generated on the core phase, enabling droplet generation with uniform size (Sattari et al., 2021). The upper limit of the $Q_{Core}$ and $Ca_{Middle}$ for the droplet generation are 0.2 µL/min and 0.7, respectively. Further, the second transition from dripping to elongation regime was then observed. The elongation regime appeared at a high $Q_{Core}$ (≥0.2 µL/min) over the wide range of the $Ca_{Middle}$. In this regime, the viscous force exerted by the middle phase at the core phase's surface is insufficient to overcome the interfacial tension, due to which, both the phases flow parallel to each other without causing droplet generation (Venkateshwarlu et al., 2021). Therefore, the low $Q_{Core}$ and $Ca_{Middle}$ are recommended to generate the w/w droplets in the microfluidic device.

## 3.3 Influence of the operating parameters on the droplets' generation

The influence of the various operating parameters such as the pressure of the valve and flow rates of the core and middle phases have been systematically explored on the droplets' generation as shown in Figure 3. In this study, 15 wt% DEX solution as a core phase, and 17 wt% PEG solution as a middle phase were used to generate the w/w droplets in the microfluidic device. As discussed above in Section 2.3, the w/w droplets were generated with the pneumatic valve, hence, the pressure of the pneumatic valve was considered to be the most important key parameter. Figure 3A presents the optical microscope (OM) images captured at the flow-focusing junction of the microfluidic device where the pressure of the valve varied from 0 to 0.4 MPa for typical flow rates of the core (0.03 µL/min) and middle (0.2 µL/min) phases. It was observed that the core phase formed a continuous thread in the middle phase with no droplet formation without a pneumatic valve (0 MPa). This confirms the pneumatic valve plays an important role in droplets' generation. When the valve was switched on and the applied pressure increased to 0.25 MPa that causes the low perturbation due to the partial squeezing and opening of the microchannel (valve switching cycle) leads to the formation of a knot-like structure or wavy interface between two phases. However, the w/w jet does not break up into droplets at

this pressure. As the pressure is increased to 0.35 MPa, due to a complete squeezing and opening of the microchannel, the w/w jet starts to break up into droplets of uniform size of 61.30 ± 3.51 μm near the flow-focusing junction. On further increasing the pressure to 0.4 MPa, the monodisperse droplet with a relatively smaller size (56.00 ± 2.11 μm) formed at the flow-focusing junction. Though, the difference is not significant as there is not much difference in the valve pressure. Further increasing the valve pressure to more than 0.4 MPa (to be more specific, 0.45 MPa) led to debonding of the microfluidic chip from the glass slide. Based on our systematic investigation of the influence of valve pressure on droplet generation, 0.35 MPa pressure was considered the optimized valve pressure and was used for further experiments and investigations.

Flow rates are crucial factors in microfluidic systems to affect the size of droplets. The effect of the different $Q_{Core}$ ranges from 0.03 to 0.3 μL/min on the droplet length (size) was examined by keeping the $Q_{Middle}$ constant (0.2 μL/min) as depicted in Figure 3B. The formation of the monodisperse spherical w/w droplets was observed at $Q_{Core}$ = 0.03 μL/min. In general, the size of the droplets increased when increasing the $Q_{Core}$. In the present study, when $Q_{Core}$ = 0.1 μL/min, the droplets squeezed in the microchannel where the length of the droplets increased may result in an increment in the size. When the $Q_{Core}$ was increased to 0.2 μL/min, more squeezing was observed increasing the length of the droplets inside the microchannel which might provide a bigger size to the droplets. The growth in droplet size occurs when there is an increase in the both inertial and viscous forces of the core phase, which indicates that more surface tension force is required to dominate inertia and viscous forces for the breakup process that can be achieved by larger droplets at the same surface tension states (Sattari et al., 2021). On further increasing the $Q_{Core}$ to 0.3 μL/min, the jetting phenomenon was observed. This validates that high valve pressure (>0.35 MPa) is required to generate the w/w droplets at the flow-focusing junction. To demonstrate the influence of $Q_{Middle}$ on droplet generation, we performed systematic experiments by varying the $Q_{Middle}$ from 0.08 to 0.8 μL/min at fixed $Q_{Core}$ at 0.03 μL/min. It can be seen from Figure 3C that the droplet size decreased with increasing $Q_{Middle}$. When the $Q_{Middle}$ = 0.08 μL/min, the w/w droplets formed from the elongated thread away from the flow-focusing junction due to the Rayleigh-Plateau instability, suggesting the surface tension is not sufficient to break up the jet into droplets at the flow-focusing junction (Rayleigh et al., 1879; Middleman, 1998; Yuen, 1968). As the $Q_{Middle}$ increased to 0.2 μL/min, the spherical droplets formed with a relatively smaller size than the droplets formed at $Q_{Middle}$ = 0.08 μL/min. On further increasing the $Q_{Middle}$ (0.5 and 0.8 μL/min), the size of the droplets decreased. This is due to the fact that increasing the $Q_{Middle}$ increases the shear force on the core phase at the flow-focusing junction and accelerates the fast detachment of the droplets from the core phase, consequently, it leads to the formation of smaller droplets (Kim et al., 2012; Sontti et al., 2019). It is apparent from Figure 3C that the increasing shear forces also caused a change in a droplet shape, increase in the droplet length confirms the increase in the shear force. We observed that the droplet generation frequency at 0.35 MPa valve pressure irrespective of the flow rates was about 3.0 Hz. Overall, the size of the droplets can be tuned by controlling the flow rates of the core and middle phases.

## 3.4 Collection of hydrogel capsules by vertical tubing and settling methods

The hydrogel capsules were fabricated *via* interfacial complexation between oppositely charged SA and chitosan polysaccharides in the microfluidic device using 0.1 wt% SA containing 15 wt% DEX solution as a core phase ($Q_{Core}$ = 0.03 μL/min), solution of 17 wt% PEG as a middle phase ($Q_{Middle}$ = 0.8 μL/min) and the shell phase comprising 0.25 wt% chitosan in 17 wt% PEG solution ($Q_{Shell}$ = 1.0 μL/min). Eventually, the SA from the core phase and chitosan from the shell phase migrate towards the middle phase, and complexation occurred *via* electrostatic interactions resulting in the formation of the hydrogel capsules with a core of DEX solution and shell composed of the SA-chitosan complexation. The resulting hydrogel capsules were collected by the conventional vertical tubing method where the Tygon tube is fixed at the outlet port as shown in Figure 4A. The OM image shows the polydisperse size of the hydrogel capsules collected from the vertical tubing method and subsequently suspended in the PBS medium (Figure 4B). The average size of the hydrogel capsules in the PBS medium was ≈304.47 μm with a large coefficient of variation (CV = 19.12%) as can be seen in the distribution graph (Figure 4C). In the case of the vertical tubing collection method, we faced three basic problems related to the collection of the hydrogel capsules. Firstly, we observed that the hydrogel capsules aggregated at the outlet port before entering the Tygon tube while moving against gravity. As a result, more pressure exerts on the capsules causes aggregation and therefore the hydrogel capsules tend to merge. Secondly, when the hydrogel capsules enter the conventional Tygon tube that has a larger diameter induces the sudden expansion of the fluid channel which decreased the flow rate of the flowing fluid, and therefore the separating distance between the hydrogel capsules decreases resulting in the aggregation and merging of the hydrogel capsules (C. Kim, Park, Kim, Jeong, & Lee, 2017). The third possible problem could be the wetting properties between the PDMS chip and plain PDMS slab, in other words, the hydrophobic nature of the PDMS walls causes aggregation which then led the merging of the capsules (which are hydrophilic). The merged microcapsule collected in the PBS medium is shown in the yellow dotted highlighted area in Figure 4B.

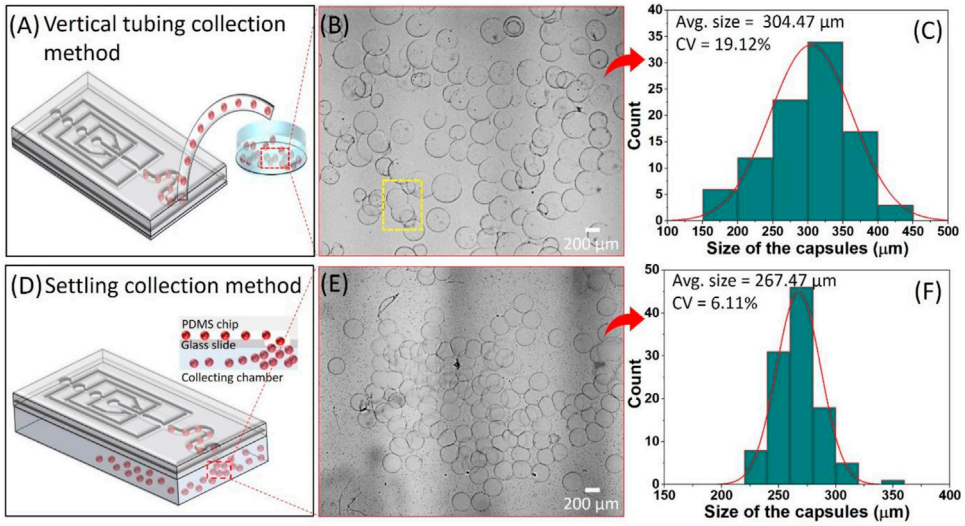


FIGURE 4
The collection of the hydrogel capsules by; **(A–C)** vertical tubing collection method, and **(D–F)** settling collection methods. **(A,D)** Schematic representation of the collection methods, **(B,E)** corresponding optical microscope image of the hydrogel capsules collected in PBS solution, and **(C,F)** size distribution graph showing the average size and coefficient of variation (CV) of the collected hydrogel capsules.

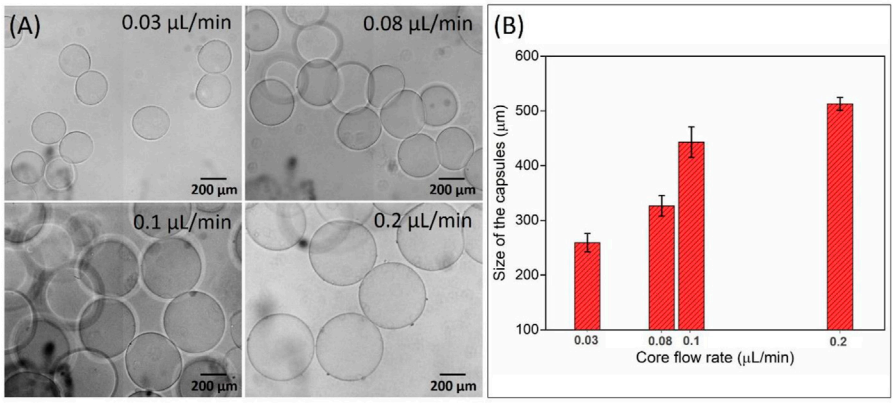


FIGURE 5
Influence of the $Q_{Core}$ on the size of the hydrogel capsules collected by the settling collection method. **(A)** Optical microscope images and **(B)** histogram of the size of hydrogel capsules as a function of different $Q_{Core}$ ranging from 0.03 to 0.2 µL/min. The $Q_{Middle}$ and $Q_{Shell}$ were kept constant at 0.8 and 1.0 µL/min, respectively.

In the case of the settling collection method, where the hydrogel capsules collected from the outlet port in the downward direction (in the direction of gravity) were settled into PBS solution as presented in Figure 4D. The OM image of the hydrogel capsules collected in the PBS solution confirms that there is no merging but aggregation was observed (Figure 4E). The aggregation is the result of the inevitable pressure difference between the inside and outside of the microfluidic device. It seems that the aggregation did not affect the intact structure of the shell of the hydrogel capsules that retained their sphericity. Also, the size distribution graph of the collected hydrogel capsules *via* the settling collection method showed the relative monodispersity with the 267.47 µm average size and with a CV of 6.11% which is three times lesser than the standard deviation of the hydrogel capsules obtained by the vertical tubing collection method (Figure 4F). Based on the above analyses, it can be concluded that the settling collection method efficiently collects the hydrogel capsules without merging problems. Further, we

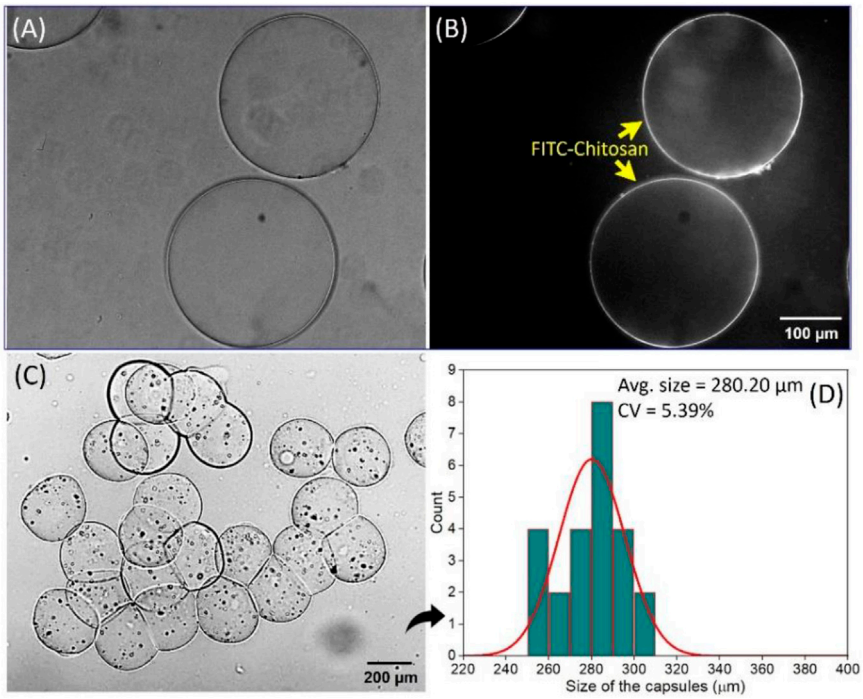


FIGURE 6
Confirmation **(A)** Bright-field image, **(B)** fluorescence image of the hydrogel capsules confirming the interfacial complexation between SA and FITC-chitosan. The encapsulation of magnetic particles, $Fe_2O_3$ nanoparticles, **(C)** optical microscope image of the hydrogel capsules encapsulating $Fe_2O_3$ nanoparticles, and **(D)** histogram of the size distribution of $Fe_2O_3$ nanoparticles encapsulated hydrogel capsules with small variation.

tuned the size of the hydrogel capsules by controlling the $Q_{Core}$ from 0.03 to 0.2 µL/min by keeping the other parameters such as $Q_{Middle}$ and $Q_{Shell}$ constant. The OM images confirm the average size of the hydrogel capsules increased with the increase of $Q_{Core}$ (Figure 5A). This result is in line with the previous reports in accordance with the general droplet microfluidic system due to the correlation between the core phase flow rate and droplet size within a certain limit (Liu et al., 2020; Wang et al., 2020). The plot of the size of the capsules as a function of different core flow rates showed the average capsule size varied from ≈260 to 510 µm by simply changing the $Q_{Core}$ from 0.03 to 0.2 µL/min (Figure 5B).

## 3.5 Confirmation and encapsulation of the hydrogel capsules

The well-defined composition, uniform size, and internal structure are the most important features of hydrogel capsules, making them ideal for encapsulating nonbiological and biological molecules (Hann et al., 2016; Perro et al., 2022). To confirm the formation of the intact shell of the hydrogel capsules *via* interfacial complexation between SA and chitosan, we first synthesized FITC-chitosan as mentioned in Section 2.4, and used it in performing the hydrogel capsule synthesis process. Further, the capsules were investigated under the optical microscope and exhibited a transparent core with a darker edge than the central part as can be seen in Figure 6A. It was then proved from the fluorescence image that the FITC-chitosan was accumulated only at the edge of the hydrogel capsules (Figure 6B). This confirms that there was no further diffusion of FITC-chitosan happened inside the capsules because of the presence of a semipermeable membrane formed after complexation between negatively charged SA and positively charged FITC-chitosan *via* electrostatic interactions at the interface. In addition, to explore the encapsulation capability of the hydrogel capsules, we used nonbiological magnetic particles, $Fe_2O_3$, and suspended them in the core phase. The compositions and flow rates are; core phase of 0.1 wt% SA containing 15 wt% DEX solution ($Q_{Core}$ = 0.03 µL/min), solution of 17 wt% PEG as a middle phase ($Q_{Middle}$ = 0.8 µL/min) and the shell phase of 0.25 wt% chitosan in 17 wt% PEG solution ($Q_{Shell}$ = 1.0 µL/min). The hydrogel capsules were collected in the PBS solution by the settling collection method. The hydrogel capsules exhibit good encapsulation capability for the $Fe_2O_3$ particles while maintaining their structural integrity as can be seen in Figure 6C. The size distribution graph shows the average size of the $Fe_2O_3$ encapsulated

hydrogel capsules was 280.20 μm and the CV of 5.39% suggesting a narrow size distribution (Figure 6D). Based on this result, we observed that the encapsulation of magnetic particles into the core phase did not affect the generation of the relatively monodisperse hydrogel capsules.

## 4 Conclusion

In summary, we designed an all-water-based microfluidic device platform for the one-step fabrication of hydrogel capsules that enabled the encapsulation of magnetic particles in a continuous process by introducing a pneumatic valve promoting droplet generation. The w/w droplet generation could be controlled by simply adjusting the pressure of the valve and flow rates of the core and middle phases. The transformation of the w/w droplets into the hydrogel capsules relies on the interfacial complexation between oppositely charged PEs, SA (polyanion), and chitosan (polycation). This microfluidic platform was further modified after its combination with the settling collection method which minimizes the coalescence between the hydrogel capsules facilitating their safe collection. The fabricated hydrogel capsules display well-defined properties of uniformity, biocompatibility, and stability which are beneficial to make them potent candidates for biomedical applications. Furthermore, we confirmed the capability of our hydrogel capsules for the encapsulation of magnetic particles, and therefore we can envision that these hydrogel capsules can be utilized in cell encapsulation and organoid construction which can be considered as our future work. Stanley, 1998, Cheung Shum et al., 2012.

## Data availability statement

The raw data supporting the conclusions of this article will be made available by the authors, without undue reservation.

## Author contributions

SD: Data curation, Formal analysis, Investigation, Methodology, Writing—original draft. JK: Formal analysis, Investigation. RG: Formal analysis, Investigation. C-SL: Conceptualization, Supervision, Validation, Writing—review and editing, Funding acquisition.

## Funding

This work was supported by the National Research Foundation of Korea (NRF) grant funded by the Korean government (the Ministry of Science and ICT) (No. 2021R1A2C3004936), the Korea Medical Device Development Fund grant funded by the Korean government (the Ministry of Science and ICT, the Ministry of Trade, Industry and Energy, the Ministry of Health and Welfare, the Ministry of Food and Drug Safety) (No. KMDF_PR_20200901_0073, 9991006746) and by National R&D Program through the NRF funded by Ministry of Science and ICT (No. 2020M3F6A1110246).

## Conflict of interest

The authors declare that the research was conducted in the absence of any commercial or financial relationships that could be construed as a potential conflict of interest.

## Publisher's note

All claims expressed in this article are solely those of the authors and do not necessarily represent those of their affiliated organizations, or those of the publisher, the editors and the reviewers. Any product that may be evaluated in this article, or claim that may be made by its manufacturer, is not guaranteed or endorsed by the publisher.

## References

Albertsson, P.-Å. (1970). Partition of cell particles and macromolecules in polymer two-phase systems. *Adv. Protein Chem.* 24, 309–341. doi:10.1016/s0065-3233(08)60244-2

Assis, R. C., Mageste, A. B., de Lemos, L. R., Orlando, R. M., and Rodrigues, G. D. (2021). Application of aqueous two-phase system for selective extraction and clean-up of emerging contaminants from aqueous matrices. *Talanta* 223 (1), 121697. doi:10.1016/j.talanta.2020.121697

Azizian, P., Azarmanesh, M., Dejam, M., Mohammadi, M., Shamsi, M., Sanati-Nezhad, A., et al. (2019). Electrohydrodynamic formation of single and double emulsions for low interfacial tension multiphase systems within microfluidics. *Chem. Eng. Sci.* 195, 201–207. doi:10.1016/j.ces.2018.11.050

Beldengrün, Y., Dallaris, V., Jaén, C., Protat, R., Miras, J., Calvo, M., et al. (2020). Formation and stabilization of multiple water-in-water-in-water (W/W/W) emulsions. *Food Hydrocoll.* 102, 105588. doi:10.1016/j.foodhyd.2019.105588

Binks, B. P. (2017). Colloidal particles at a range of fluid-fluid interfaces. *Langmuir* 33 (28), 6947–6963. doi:10.1021/acs.langmuir.7b00860

Buzza, D. M., Fletcher, P. D., Georgiou, T. K., and Ghasdian, N. (2013). Water-in-water emulsions based on incompatible polymers and stabilized by triblock copolymers-templated polymersomes. *Langmuir* 29 (48), 14804–14814. doi:10.1021/la403356j

Chao, Y., and Shum, H. C. (2020). Emerging aqueous two-phase systems: From fundamentals of interfaces to biomedical applications. *Chem. Soc. Rev.* 49 (1), 114–142. doi:10.1039/c9cs00466a

Cheung Shum, H., Varnell, J., and Weitz, D. A. (2012). Microfluidic fabrication of water-in-water (w/w) jets and emulsions. *Biomicrofluidics* 6 (1), 012808–128089. doi:10.1063/1.3670365

Daradmare, S., and Lee, C. S. (2022). Recent progress in the synthesis of all-aqueous two-phase droplets using microfluidic approaches. *Colloids Surfaces B Biointerfaces* 219, 112795. doi:10.1016/j.colsurfb.2022.112795

Dumas, F., Benoit, J. P., Saulnier, P., and Roger, E. (2021). A new method to prepare microparticles based on an Aqueous Two-Phase system (ATPS), without organic solvents. *J. Colloid Interface Sci.* 599, 642–649. doi:10.1016/j.jcis.2021.03.141

Ferreira-Faria, D., Aires-Barros, M. R., and Azevedo, A. M. (2020). Continuous aqueous two-phase extraction: From microfluidics to integrated biomanufacturing. *Fluid Phase Equilibria* 508, 112438. doi:10.1016/j.fluid.2019.112438

Hann, S. D., Niepa, T. H., Stebe, K. J., and Lee, D. (2016). One-step generation of cell-encapsulating compartments via polyelectrolyte complexation in an aqueous two phase system. *ACS Appl. Mat. Interfaces* 8 (38), 25603–25611. doi:10.1021/acsami.6b07939

Hann, S. D., Stebe, K. J., and Lee, D. (2017). All-aqueous assemblies via interfacial complexation: Toward artificial cell and microniche development. *Langmuir* 33 (39), 10107–10117. doi:10.1021/acs.langmuir.7b02237

Jang, S., Lee, B., Jeong, H. H., Jin, S. H., Jang, S., Kim, S. G., et al. (2016). On-chip analysis, indexing and screening for chemical producing bacteria in a microfluidic static droplet array. *Lab. Chip* 16 (10), 1909–1916. doi:10.1039/c6lc00118a

Jin, S. H., Lee, B., Kim, J. S., and Lee, C.-S. (2021). Improvement strategy of a microfluidic sorter using a pneumatic bilayer valve. *Chem. Eng. Sci.* 245, 116834. doi:10.1016/j.ces.2021.116834

Kim, B. I., Jeong, S. W., Lee, K. G., Park, T. J., Park, J. Y., Song, J. J., et al. (2012). Synthesis of bioactive microcapsules using a microfluidic device. *Sensors (Basel)* 12 (8), 10136–10147. doi:10.3390/s120810136

Kim, C., Park, K.-S., Kim, J., Jeong, S.-G., and Lee, C.-S. (2017). Microfluidic synthesis of monodisperse pectin hydrogel microspheres based on *in situ* gelation and settling collection. *J. Chem. Technol. Biotechnol.* 92 (1), 201–209. doi:10.1002/jctb.4991

Kim, D. Y., Jin, S. H., Jeong, S. G., Lee, B., Kang, K. K., and Lee, C. S. (2018). Microfluidic preparation of monodisperse polymeric microspheres coated with silica nanoparticles. *Sci. Rep.* 8 (1), 8525. doi:10.1038/s41598-018-26829-z

Liu, H., Wang, Y., Wang, H., Zhao, M., Tao, T., Zhang, X., et al. (2020). A droplet microfluidic system to fabricate hybrid capsules enabling stem cell organoid engineering. *Adv. Sci. (Weinh).* 7 (11), 1903739. doi:10.1002/advs.201903739

Ma, Q., Song, Y., Kim, J. W., Choi, H. S., and Shum, H. C. (2016). Affinity partitioning-induced self-assembly in aqueous two-phase systems: Templating for polyelectrolyte microcapsules. *ACS Macro Lett.* 5 (6), 666–670. doi:10.1021/acsmacrolett.6b00228

Navi, M., Kieda, J., and Tsai, S. S. H. (2020). Magnetic polyelectrolyte microcapsules via water-in-water droplet microfluidics. *Lab. Chip* 20 (16), 2851–2860. doi:10.1039/d0lc00387e

Palogan, B., Kumar, R., and Bhattacharya, S. (2020). Effect of surface coating on droplet generation in flow-focusing microchannels. *Microfluid. Nanofluidics* 24 (9), 72. doi:10.1007/s10404-020-02380-0

Perro, A., Coudon, N., Chapel, J. P., Martin, N., Beven, L., and Douliez, J. P. (2022). Building micro-capsules using water-in-water emulsion droplets as templates. *J. Colloid Interface Sci.* 613, 681–696. doi:10.1016/j.jcis.2022.01.047

Rayleigh, L. (1879). On the capillary phenomena of Jets. *Proc. R. Soc. Lond.* 29, 71–97. doi:10.1098/RSPL.1879.0015

Sattari, A., Janfaza, S., Mashhadi Keshtiban, M., Tasnim, N., Hanafizadeh, P., and Hoorfar, M. (2021). Microfluidic on-chip production of alginate hydrogels using double coflow geometry. *ACS Omega* 6 (40), 25964–25971. doi:10.1021/acsomega.1c02728

Sauret, A., Spandagos, C., and Shum, H. C. (2012). Fluctuation-induced dynamics of multiphase liquid jets with ultra-low interfacial tension. *Lab. Chip* 12 (18), 3380–3386. doi:10.1039/c2lc40524e

Sharma, K., Somavarapu, S., Colombani, A., Govind, N., and Taylor, K. M. (2012). Crosslinked chitosan nanoparticle formulations for delivery from pressurized metered dose inhalers. *Eur. J. Pharm. Biopharm.* 81 (1), 74–81. doi:10.1016/j.ejpb.2011.12.014

Song, Y. S., Choi, Y. H., and Kim, D. H. (2007). Microextraction in a tetrabutylammonium bromide/ammonium sulfate aqueous two-phase system and electrohydrodynamic generation of a micro-droplet. *J. Chromatogr. A* 1162 (2), 180–186. doi:10.1016/j.chroma.2007.06.032

Sontti, S. G., and Atta, A. (2019). Numerical insights on controlled droplet formation in a microfluidic flow-focusing device. *Ind. Eng. Chem. Res.* 59 (9), 3702–3716. doi:10.1021/acs.iecr.9b02137

Stanley, M. (1998). *An introduction to fluid dynamics*. Hoboken, New Jersey: John Wiley.

Venkateshwarlu, A., and Bharti, R. P. (2021). Effects of capillary number and flow rates on the hydrodynamics of droplet generation in two-phase cross-flow microfluidic systems. *J. Taiwan Inst. Chem. Eng.* 129, 64–79. doi:10.1016/j.jtice.2021.07.045

Wang, Y., Liu, H., Zhang, M., Wang, H., Chen, W., and Qin, J. (2020). One-step synthesis of composite hydrogel capsules to support liver organoid generation from hiPSCs. *Biomater. Sci.* 8 (19), 5476–5488. doi:10.1039/d0bm01085e

Yuen, M. C. (1968). Non-linear capillary instability of a liquid jet. *J. Fluid Mech.* 33 (1), 151–163. doi:10.1017/S0022112068002429

Zhang, L., Cai, L. H., Lienemann, P. S., Rossow, T., Polenz, I., Vallmajo-Martin, Q., et al. (2016). One-step microfluidic fabrication of polyelectrolyte microcapsules in aqueous conditions for protein release. *Angew. Chem. Int. Ed.* 55 (43), 13470–13474. doi:10.1002/anie.201606960

Ziemecka, I., Steijn, V., Koper, G. J. M., Kreutzera, M. T., and Van Esch, J. H. (2011). All-aqueous core-shell droplets produced in a microfluidic device. *Soft Matter* 7 (21), 9878–9880. doi:10.1039/C1SM06517C

Zou, Y., Song, J., You, X., Yao, J., Xie, S., Jin, M., et al. (2019). Interfacial complexation induced controllable fabrication of stable polyelectrolyte microcapsules using all-aqueous droplet microfluidics for enzyme release. *ACS Appl. Mat. Interfaces* 11 (23), 21227–21238. doi:10.1021/acsami.9b02788